RSC Advances

ROYAL SOCIETY OF CHEMISTRY

www.rsc.org/advances

RSC Advances

RSC Advances

ARTICLE

Heterogeneous activation of hydrogen peroxide by γ-Al_2O_3 supported bimetallic Fe, Mn for the degradation of Reactive Black 5

Cite this: DOI:

Received,
Accepted

DOI:

www.rsc.org/

Yan Wang[a,b], Jianfei Wang[a,b,†], Haimin Zou[a,b], Yue Xie[a,b]

Abstract: Fe-Mn/γ-Al_2O_3 catalyst was prepared by wet impregnation method and used for the degradation of Reactive black 5 (RB5) as an activator of hydrogen peroxide (H_2O_2). The prepared catalyst was characterized with XRD, FTIR and SEM-EDS. The results showed that Al_2O_3 could effectively restrain Fe and Mn. The catalytic activity of Fe-Mn/γ-Al_2O_3 was significantly higher than that of pure γ-Al_2O_3, Fe/γ-Al_2O_3, and Mn/γ-Al_2O_3. After four reuses, Fe-Mn/γ-Al_2O_3 maintained high catalytic activity and approximately 98% of the color removal was reached after 75 min reaction. Effects of important operational parameters such as initial pH of solution, H_2O_2 amount, and catalyst addition on the decolorization efficiency were investigated. The results displayed that the RB5 discoloration efficiency increased firstly and then decreased with increasing H_2O_2 concentration and pH, as well as increased firstly and then maintained stability with increasing catalyst addition. The best decolorization efficiency (98.02%) was obtained at pH = 3, H_2O_2 amount = 7 mmol L^{-1}, catalyst addition = 2.5 g L^{-1} for initial RB5 concentration of 50 mg/L. Finally, the TOC removal was only 39.60% after 75 min reaction, prolonging the reaction time to 160 min, 62.23% of TOC removal efficiency could be achieved under the optimal operational parameters.

Keywords: Reactive black 5; Degradation; Heterogeneous Fenton reaction; Fe-Mn/Al_2O_3

1. Introduction

In recent years, the pollution of water resources by huge amount of dye wastewater generated from textile dyeing, leather, paper, pharmaceutical and food industry, which has become a serious environmental problem and has attracted increasing attention.[1-3] Because dye wastewater contains many kinds of hazardous organic compounds, which are highly soluble in water and difficult to degradation by biological treatment processes.[4,5] Moreover, more than 50% of dyes used in the textiles industries is azo dyes, characterised by one or more azo bonds (–N=N–) in association with one or more aromatic systems and auxochromes (–OH, $–SO_3$, etc.).[3,6-7] The azo group is responsible for producing the colour while auxochromes enhance the affinity of the dye towards water,[8,9] which would resulted in high dye concentration and strong biological toxicity. However, the organics in dye wastewaters from dyeing and related industries cannot be effectively treated by conventional biological processes due to biological toxicity of these pollutants.[10-12] In order to comply with environmental regulations, it is important and urgent to dispose dye wastewater in a proper and efficiency way.

Advanced oxidation processes (AOPs), based on generation and utilization of reactive species, are considered as one of the most effective and promising methods for degradation of toxic and/or bio-refractory organic pollutants in wastewater and have received the increasing attention.[13,14] Hydroxyl radicals (•OH), one of reactive species, have a high standard oxidation potential and react none selectively as well as are concerned by many researchers.[13-15] Among AOPs, H_2O_2 as one of powerful oxidants, has been used for the degradation of dye wastewater in presence of transition metal salt or oxides.[2-3,16-17] Compared with metal salt, metal oxides are the better candidate for the practical application in wastewater treatment due to their easily separation. Particularly, Fe-containing oxide catalysts have been investigated widely for chemical activation of H_2O_2 due to their friendly to environment and inexpensive operating cost, such as goethite,[3,16-17] α-Fe_2O_3,[18] $CuFeO_2$,[15] $LaFeO_3$[19] and $BiFeO_3$[19] . However, many catalysts showed difficulty for recovery or low activities or strong iron leaching due to low pH, which resulted in secondary pollution.[20,21] Among various transition metal catalysts, Mn was considered as a promising candidate due to the reason that Mn-containing oxide catalysts had several features,[22] such as (i) remarkable catalytic performances for the decomposition of H_2O_2 in aqueous solution to produce •OH,[23,24] (ii) Mn(II) could enhance the catalytic oxidation of Fe(III)/H_2O_2 system.[25,26] Therefore, Fe and Mn bimetallic catalyst were introduced to overcome the drawback of Fe containing oxide catalysts and improve the utilization of Fe containing oxide catalysts.[27,28]

However, the effective approaches for their aggregation are the bottleneck for their practical applications.[21] Thus, to its aggregation, Fe and Mn bimetallic metal oxides are usually deposited on a solid support with a larger surface area. Al_2O_3 as a solid support of catalyst has been used for advanced oxidation of organic pollutants due to their abundant, inexpensive, environmentally friendly and high surface area. [29-32] Although many dispersed states of a supported single metal oxide were reported,[30-32] there was little literatures about supported dual metal oxides as heterogeneous Fenton catalyst for the degradation of azo dye.[5,27,33]

Herein, the supported dual metal oxides Fe-Mn/γ-Al_2O_3 was prepared as heterogeneous Fenton catalyst for the degradation of azo dye Reactive Black 5 (RB5) in this study. The catalyst was characterized by X-ray diffraction (XRD), fourier transform infrared spectrometer (FTIR) and scanning electron microscope (SEM). The efficiency and stability of Fe-Mn/γ-Al_2O_3 for the degradation of RB5

dye in a heterogeneous system were evaluated. The mineralization of RB5 in terms of total organic carbon (TOC) removal and the effects of operating conditions such as Fe-Mn/γ-Al_2O_3 addition rate, H_2O_2 concentration and initial pH on color removal were analyzed.

2. Experiment

2.1 Materials

Reactive black 5 (RB5) was purchased from Shanghai Shiyi Chemicals Reagent Co. Ltd. (China) and used as received. Hydrogen peroxide (analytical, grade, 30%, w/w), $MnSO_4$ and $FeCl_3$ were obtained from Shanghai Sinopharm Chemical Reagent Co., Ltd and used as received. γ-Al_2O_3 powder was obtained from Shanghai Sinopharm Chemical Reagent Co., Ltd and before use. All solution was prepared with deionized water.

2.2 Catalyst preparation and oxidation procedure

The catalyst was prepared by a wet impregnation method.[34] 1 g γ-Al_2O_3 supporter was placed in 500 mL beaker with containing 250 mL mixed solution consisted of 0.05 mol L^{-1} $MnSO_4$ and/or 0.05 mol L^{-1} $FeCl_3$. The mixed solution was kept at room temperature under magnetic stirring for 24 h. Then the mixed solution was filtered through 0.45 μm membranes, and the solid was washed with deionized water to neuter. Then the solid material was dried at 110ºC for 2 h under vacuum conditions. Finally, the collected powder was calcined in a muffle furnace at 450ºC for 3 h and Fe-Mn/γ-Al_2O_3 was obtained.

In all experiments, a stock solution of RB5 was prepared fresh before each run and the initial RB5 concentration was kept at 50 mg L^{-1}. The solution pH was measured with a Mettler Toledo FE20 pH-meter. Batch experiments were performed in the glass reactor containing 200 mL solution, which was similar to our previous study.[3] A given amount of H_2O_2 and Fe-Mn/γ-Al_2O_3 were added simultaneously into the reactor. A magnetic stirrer provided complete mixing of the solution in the reactor. At pre-selected time intervals, samples were removed by a syringe and filtered through 0.22 μm membranes before the RB5 concentration was measured.

2.3 Analysis methods

The absorbance of RB5 was measured at λ_{max} = 591 nm using a Shimadzu UV-1700 spectrophotometer. Total organic carbon (TOC) was analyzed using a TOC analyzer (Shimadzu TOC-L) to evaluate the mineralization of RB5.

The leaching concentrations of Fe and Mn were determined by an atomic absorption spectrophotometer (AAS, ZEEnit700). The concentration of H_2O_2 was determined by titanium oxalate spectrophotometric method.[3,35-36]

The morphology of the catalyst were carried out using a scanning electron microscope with energy dispersive spectra for the atomic composition of catalyst surface (SEM-EDS, Zeiss EVO LS-185, The England). X-ray diffraction (XRD) patterns were recorded on a D/Max-2550 PC diffractometer in θ–2θ configuration to identify the crystal phase and structure. The wide angle data were collected from 20◦ to 90◦ on 2θ scale,when the operated condition was set at 36 kV/24 mA, using $Cu_{K\alpha1}$ radiation with a wavelength of 1.5406Å.

The infrared spectra of synthesized Fe-Mn/γ-Al_2O_3 were recorded on KBr pellets by a Fourier transform infrared spectrometer (FTIR, Nicolet Avatar 330). To avoid moisture, KBr pellets were prepared by pressing mixtures of dry powered sample and spectrometry-grade KBr under vacuum. 150 scans were collected for each sample in the range of 400–4000 cm^{-1} with a resolution of 2 cm^{-1}.

3. Results and discussion

3.1 Characterization and stability of synthesized Fe-Mn/γ-Al_2O_3

The XRD analysis is applied to define the structure of γ-Al_2O_3 carrier and Fe-Mn/γ-Al_2O_3 as well as the obtained patterns are shown on Fig. 1a. It is obvious that γ-Al_2O_3 and Fe-Mn/γ-Al_2O_3 exhibit similar XRD patterns. It also can be seen from Fig.1a that commercial γ-Al_2O_3 support showed the typical diffraction peaks (111), (311),(400) and (440) of γ-Al_2O_3 with a cubic structure[30,37-38] and the characteristic peaks of γ-Al_2O_3 at about 38°, 46°, and 67°.[39] After iron and manganese doping, although the structure of γ-Al_2O_3 remained intact, the intensities of all these peaks decreased slightly, implying the interaction among iron and manganese and γ-Al_2O_3. Iron and manganese are present in γ-Al_2O_3 as their oxides under high temperature calcination. The Fe–Mn binary oxide particles showed no notable peaks, indicating that no crystalline phase was present and the Fe–Mn binary oxide particles was too little to cause significant changes of XRD peaks.

Fig.1.

The FTIR spectra of powder samples are shown in Fig. 1b. There is signature of two important bands below 1000 cm^{-1} in the FTIR spectra. The peak around 540 cm^{-1} corresponds to vibration of octahedral manganese–oxygen (Mn–O) bonds and the absorption peak at 1058 cm^{-1} can be possibly attributed to Mn^{3+}–O vibration.[40-42] The band at 1630 $cm^{-1}$was assigned to the bending vibration of the O–H bonded with Mn atoms.[40,43] Meanwhile, the absorption peaks at 585 cm^{-1} is assigned to the presence of typical tetrahedral stretching characteristic of ferrites when 1360 cm^{-1} reflects the octahedral sites of ferrites.[40,44-46] The wide band at 3435 cm^{-1} was attributed to the stretching and bending vibrations of water molecules and hydroxyl groups.[40,45,47]

SEM images of γ-Al_2O_3 (Fig. 1c) showed a cubic structure and smooth surface. However, SEM photos of Fe-Mn/γ-Al_2O_3 (Fig. 1c) not just showed a cubic structure but also exhibited rough surface and bright zones which were confirmed by EDS to be due to local Fe and Mn content. The quantitative surface chemical compositions are presented in Table 1. The loading amount of Fe and Mn are 7.45 mol% and 3.05 mol%, respectively, which is proved that Fe and Mn are covered on the surface of γ-Al_2O_3.

Table1

3.2 Decolorization of RB5 under different systems

To evaluate the decolorization efficiency of RB5 under differentsystems, H_2O_2, γ-Al_2O_3, Fe/γ-Al_2O_3, Mn/γ-Al_2O_3, Fe-Mn/γ-Al_2O_3, γ-Al_2O_3/H_2O_2, Fe/γ-Al_2O_3/H_2O_2, Mn/γ-Al_2O_3/H_2O_2, Fe-Mn/γ-Al_2O_3/H_2O_2 for the decolorization efficiency were conducted and the result was shown in Fig.2a. It can be seen that the decolorization efficiency observed was 10.65, 11.78, and 10.79% when adding into the RB5 solution with γ-Al_2O_3, Fe/γ-Al_2O_3 and Mn/γ-Al_2O_3 alone, respectively. Compared with γ-Al_2O_3, Fe/γ-Al_2O_3 or Mn/γ-Al_2O_3, the decolorization efficiency of the RB5 solution increased slightly with Fe-Mn/γ-Al_2O_3 alone and was 16.89%, indicating the effect of adsorption on RB5 decolorization was not notable under the condition investigated.

Negligible decolorization also occurred when H_2O_2 alone was applied due to its limited oxidation power (E^0 = 1.78 V) [3,48] and there were 96.02% of H_2O_2 after 75 min reaction in the reaction solution (Fig. 2b), indicating little of H_2O_2 was decomposed in this case. The RB5 removal was only 27% in γ-Al_2O_3/H_2O_2 process and

the remaining percentage of H_2O_2 was 92.04%. This may due to the weak catalytic activity of γ-Al_2O_3 for H_2O_2 decomposition. However, both of Fe/γ-Al_2O_3 and Mn/γ-Al_2O_3 could catalyze H_2O_2 to generate $^{\bullet}OH$, resulting in 80.59% and 90.95% of decolourization efficiency after 75 min reaction through Eqs. (1) and (2):[19,28,30,49-50]

$$\equiv Fe^{2+} + H_2O_2 \rightarrow \equiv Fe^{3+} + {}^{\bullet}OH + OH^- \quad (1)$$

$$\equiv Mn^{2+} + H_2O_2 \rightarrow \equiv Mn^{3+} + {}^{\bullet}OH + OH^- \quad (2)$$

where the symbol ≡ represents the metal species bound to the surface of the catalyst. Simultaneously, 67.82% and 59.63% were decomposed in Fe/γ-Al_2O_3/H_2O_2 system and Mn/γ-Al_2O_3/H_2O_2 system, respectively. The RB5 decolorization efficiency increased to 98.02% and the remaining percentage of H_2O_2 was 42% in Fe-Mn/γ-Al_2O_3/H_2O_2 process. Compared with Mn/γ-Al_2O_3 and Fe/γ-Al_2O_3, the RB5 decolorization rate is higher in Fe-Mn/γ-Al_2O_3/H_2O_2 process, indicating the catalytic activity of Fe-Mn/γ-Al_2O_3 was much greater. It is due to two reasons: (i) both of ≡Fe(II) and ≡Mn(II) can react with H_2O_2 to generate active radicals, (ii) ≡Mn(III) produced during the reaction process can accelerate the production of $^{\bullet}OH$ as the following Eqs.(3)-(5)[25,51] and Eq.(1),

$$\equiv Mn(III) + H_2O_2 \rightarrow \equiv MnO_2^+ + 2H^+ \quad (3)$$

$$\equiv MnO_2^+ + H^+ \rightarrow HO_2^{\bullet}/O_2^{\bullet-} + \equiv Mn(II) \quad (4)$$

$$HO_2^{\bullet-} + \equiv Fe(III) \rightarrow \equiv Fe(II) + H^+ + O_2 \quad (5)$$

According to Eqs.(1)-(5), ≡Mn(III) promotes the production of $HO_2^{\bullet-}/O_2^{\bullet-}$ through a series of reactions involved manganese species, $^{\bullet}OH$, $HO_2^{\bullet-}/O_2^{\bullet-}$ and H_2O_2. Then, $HO_2^{\bullet-}/O_2^{\bullet-}$ reacts with ≡Fe(III) to accelerate the formation of ≡Fe(II), and finally accelerates the production of $^{\bullet}OH$ and the degradation of RB5.

Fig.2.

3.3 Stability of Fe-Mn/γ-Al_2O_3 catalyst during the heterogeneous activation process

The stability of catalyst is as important as its catalytic activity. Therefore, in order to confirm the stability of Fe-Mn/γ-Al_2O_3, the recycle experiments were performed when the pH was 3, Fe-Mn/γ-Al_2O_3 addition was 2.5 g L^{-1}, the RB5 concentration was 50 mg L^{-1} and the H_2O_2 concentration was 7 mmol L^{-1}. The experiment of the catalytic degradation of RB5 was repeated for four cycles and each experiment was lasted for 75 min. The catalyst was easily removed from the reactor after each repetitive oxidation process, then washed by deionized water, dried in the vacuum oven, calcined in the muffle furnace and stored at ambient temperature. As shown in Fig.3a, the removal efficiencies of RB5 during four reaction cycles were 98.02%, 98.06%, 97.95%, and 97.86%, respectively. The decolorization efficiencies of RB5 are nearly the same in four successive cycles and the remaining percentages of H_2O_2 in each recycle experiment were similar (Fig. 3b). The metal leaching level was not obviously changed after four recycle time, with the Fe content in the solution at the end of the test almost constant at 0.15–0.23 mg L^{-1} as the Mn content at 0.07–0.13 mg L^{-1}. These indicate Fe-Mn/γ-Al_2O_3 is an excellent long-term stable catalyst for the Fe-Mn/γ-Al_2O_3/H_2O_2 system.

Fig.3.

3.4 Effect of initial pH on the RB5 decolorization

The comparison of RB5 decolorization efficiency under different initial pH was investigated with Fe-Mn/γ-Al_2O_3 addition 2.5 g L^{-1}, the RB5 concentration 50 mg L^{-1} and the H_2O_2 concentration 7 mmol L^{-1}. As can be seen from Fig.4a, the decolorization efficiency increased from 87.00% to 98.02% as the initial pH value increased from 2 to 3. When pH value was below 3, the solution provided a large number of hydrogen ions for H_2O_2 transformation into more stable oxoniumion $H_3O_2^+$,[3,52-53]

$$H_2O_2 + H^+ \rightarrow H_3O_2^+ \quad (6)$$

On the other hand, hydrogen ion would act as the scavenger of hydroxyl radicals at a very low pH,[3,54-55]

$$^{\bullet}OH + H^+ + e^- \rightarrow H_2O \quad (7)$$

where electrons may be gained from ferrous ions.[55] Moreover, hydrogen ions could restrain the formation of ≡Fe(II) through Eqs. (3) and (5), resulting in the generation of $^{\bullet}OH$. Therefore, the decolorization rate decreased as the pH dropped from 3 to 2.

The decolorization efficiency decreased from 98.02% to 30.92% when the initial pH value increased from 3 to 9. Based on Eqs. (1) and (2), OH^- increased with the improvement of the initial pH, which would inhibit the $^{\bullet}OH$ generation proved from the remaining percentages of H_2O_2 (Fig.4b). Interestingly, Fe-Mn/γ-Al_2O_3 exhibited certain catalytic activity when pH changed from 2 to 9. Compared with Fe-RHA,[56] Fe-Mn/γ-Al_2O_3 demonstrated higher catalytic active in wide range of pH.

Fig.4.

3.5 Effect of H_2O_2 concentration on the RB5 decolorization

As the source of hydroxyl radicals, H_2O_2 plays a significant role in Fe-Mn/γ-Al_2O_3/H_2O_2 process, the effect of the H_2O_2 concentration on the degradation of RB5 was also explained by varying the concentration of H_2O_2 from 1.75 to 10.50 mmol L^{-1}, when the pH was 3, Fe-Mn/γ-Al_2O_3 addition was 2.5 g L^{-1} and the RB5 concentration was 50 mg L^{-1}, and the result was depicted in Fig.5a.

As shown in Fig.5a, when H_2O_2 concentration increased from 1.75 to 7.00 mmol L^{-1}, the RB5 decolorization efficiency increased from 49.92% to 98.02%. Meanwhile, the amount of decomposed H_2O_2 also increased in Fig.5b, indicating more reactive radicals would be generated to degrade RB5 at higher H_2O_2 concentration. However, the further increase in H_2O_2 concentration resulted in a decrease of RB5 degradation rates when the H_2O_2 concentration reached 7.00 mmol L^{-1}. This is due to the fact that H_2O_2 is both of the source and the inhibitor for $^{\bullet}OH$, excess H_2O_2 competed with organic compound for $^{\bullet}OH$ and consumed $^{\bullet}OH$.[19,57] The similar phenomenon was reported by Amorim et al when they degraded the azo anionic dye Reactive Red 195 with photo-Fenton-like processes.[58] Therefore, 7.00 mmol L^{-1} was selected as the optimal initial H_2O_2 concentration and used in the following experiments.

Fig.5.

3.6 Effect of catalyst dosage on the RB5 decolorization

The addition dosage of the catalyst would influence the decolorization significantly because the catalyst is the source of ≡Fe(II) and ≡Mn(II) which are the major species that could activate H_2O_2 to generate $^{\bullet}OH$.[3,19,59] The decolorization of RB5 was investigated at different dosages of Fe-Mn/γ-Al_2O_3 catalyst when initial pH was 3, the RB5 concentration was 50 mg L^{-1} and the H_2O_2 concentration was 7 mmol L^{-1}. As can be seen in Fig. 6a, the decolorization efficiency of RB5 significantly increased from 59.74 to 98.02% after 75 min reaction when Fe-Mn/γ-Al_2O_3 addition increased from 0.5 to 2.5 g L^{-1}. The increase of Fe-Mn/γ-Al_2O_3 dosage corresponds to the increase of the total specific area and active sites, resulting in the faster H_2O_2 decomposition to generate more $^{\bullet}OH$.[58,59] Thus, the remaining percentages of H_2O_2 decreased in Fig. 6b and the removal rate of RB5 was enhanced with increasing Fe-Mn/γ-Al_2O_3 dosage. Although the increase of Fe-Mn/γ-Al_2O_3 dosage resulted in the increase of decolorization rate, the decolorization efficiency after 75 min reaction was nearly the same at the fixed H_2O_2 concentration, which was approximately 98% as illustrated in Fig. 6a. Because the increasing Fe-Mn/γ-Al_2O_3 dosage

could only increase the generated $^{\bullet}OH$ rate and could not improve the amount of generated $^{\bullet}OH$ which was only dependent on H_2O_2 dosage. However, 7 mmol L^{-1} H_2O_2 was sufficient to generate $^{\bullet}OH$ when only decolorization was concerned.

Fig.6.

3.7 The decolorization and mineralization of RB5 with reaction time

As is known to all, complete decolorization of dye did not mean that the dye was completely oxidized to CO_2, H_2O, and so on.[3,60] According to the previous reports,[55, 61] the only decolorization of RB5 could be described by equation below,

$$C_{26}H_{21}N_5Na_4O_{19}S_6 + {}^{\bullet}OH \rightarrow C_{26}H_{21}N_5Na_4O_{19}S_6(\text{—}OH) + \text{oxidized intermediates} + CO_2 \quad (8)$$

On the basis of this equation, there were only 0.05 mmol L^{-1} of H_2O_2 theoretically for complete decolorization of 50 mg L^{-1} RB5. But when mineralization was concerned, the following mechanism could be suggested for the decomposition of RB5,

$$C_{26}H_{21}N_5Na_4O_{19}S_6 + 82.5H_2O_2 \rightarrow 26CO_2 + 93H_2O + 5NO_3^- + 6SO_4^{2-} + Na^+ \quad (9)$$

Then 4.16 mmol L^{-1} of H_2O_2 were theoretically needed to completely decompose 50 mg L^{-1} RB5, which would be much more than that needed to completely bleach RB5. Thus, the mineralization of RB5 in terms of TOC removal was investigated. As can be seen in Fig. 7, the mineralization of RB5 was investigated by Fe-Mn/γ-Al_2O_3/H_2O_2 process. Though the decolorization efficiency could reach 98.02% after 75 min reaction, only 39.60% TOC removal was obtained. This indicated most of RB5 was converted to smaller intermediates. When the reaction time was prolonged to 160 min, 62.23% of TOC removal efficiency could be achieved when the H_2O_2 concentration was 7 mmol L^{-1} which was much more than theoretical H_2O_2 concentration 4.16 mmol L^{-1}. Therefore it could be expected that more aggressive conditions and more reaction time are required to achieve higher TOC removal than those employed to simply break the chromophore group.

Fig.7.

4. Conclusions

This study showed that the heterogeneous activation process is effective for the decolorization of RB5. The bimetallic Fe-Mn/γ-Al_2O_3 catalyst behaves as efficient and stable catalyst for the heterogeneous oxidation of RB5. The optimal conditions for efficient RB5 degradation were pH 3, H_2O_2 concentration 7 mmol L^{-1}, and catalyst loading 2.5 g/L. Under the conditions above, the decolorization efficiency was 98.02% after 75 min reaction and TOC removal was 62.23% within 160 min. Consequently, the coupled Fe-Mn/γ-Al_2O_3/H_2O_2 system appears as a promising process for the dye wastewater treatment.

Acknowledgements

This work was supported by Natural Science Foundation of Anhui Province, China (Grant 1508085ME90, 1508085QD74) and Natural science research project of Anhui Province, China (Grant KJ2015A188, KJ2015A195).

Notes references

[a] Department of Environmental science and Engineering, Anhui Science and Technology University, Donghua Road 9#, Fengyang 233100, China

b Key Laboratory of Bioorganic Fertilizer Creation, Ministry of Agriculture, Bengbu 234000, China

† Corresponding author. Tel.: +86 550 6732317; fax: +86 550 6732317; E-mail address: E-mail: jykwjf@sina.com.

Reference

1 C. Cai, L.G. Wang, H. Gao, L.W. Hou and H. Zhang, *J. Environ. Sci.*, 2014, **26**, 1267–1273.
2 T.D. Nguyen, N.H. Phan, M.H.Do and K.T. Ngo, *J. Hazard. Mater.*, 2011, **185**, 653–661.
3 Y. Wang, Y.W. Gao, L. Chen and H. Zhang, *Catal. Today*, 2015, **252**, 107–112.
4 Y.W. Gao, Y. Wang and H. Zhang, *Appl. Catal. B: Environ.*, 2015, **178**, 29–36.
5 Y. Liu and D.Z. Sun, *J. Hazard. Mater.*, 2007, **143**, 448–454.
6 H. Lin, H. Zhang, X. Wang, L.G. Wang and J. Wu, *Sep. Purif. Technol.* 2014, **122** , 533–540.
7 M. Dükkanci, M. Vinatoru and T.J. Mason, *Ultrason. Sonochem.,* 2014, **21**, 846–853.
8 L. Doumic, G. Salierno, M. Cassanello, P. Haure and M. Ayude, *Catal. Today*, 2015, **240**, 67–72.
9 L. Zhang, Z.J. Cheng, X. Guo, X.H. Jiang and R. Liu, *J. Mol. Liq.*, 2014, **197**, 353–367.
10 E. Saputra, S. Muhammad, H.Q. Sun, H.M. Ang, M.O. Tadé and S.B. Wang, *Appl. Catal. B: Environ.*, 2013, **142–143**, 729–735.
11 L.A.V. de Luna, T.H.G. da Silva, R.F.P. Nogueira, F. Kummrow and G.A. Umbuzeiro, *J. Hazard. Mater.*, 2014, **276**, 332–338.
12 V. Dulman, S.M. Cucu-Man, R.I. Olariu, R. Buhaceanu, M. Dumitraş and Ion Bunia, *Dyes Pigments*, 2012, **95**, 79-88.
13 C.G. Niu, Y. Wang, X.G. Zhang, G.M. Zeng, D.W. Huang, M. Ruan and X.W. Li, *Bioresource Technol*., 2012, **126**, 101–106.
14 A. El-Ghenymy, F. Centellas, J.A. Garrido, R.M. Rodríguez, I.Sirés, P.L. Cabot and E. Brillas, *Electrochim. Acta*, 2014, **130**, 568–576.
15 X.Y. Zhang, Y.B. Ding, H.Q. Tang, X.Y. Han, L.H. Zhu and N. Wang, *Chem. Eng. J.*,2014, **236**, 251–262.
16 H.H. Wu, X.W. Dou, D.Y. Deng, Y.F. Guan, L.G. Zhang and G.P. He, *Environ. Technol.*, 2012, **33**, 1545–1552.
17 J. He, W.H. Ma, W.J. Song, J.C. Zhao, X.H. Qian, S.B. Zhang and J.C. Yu, *Water Res*. 2005, **39**, 119–128.
18 G.M.S. ElShafei, F.Z. Yehia, O.I.H. Dimitry, A.M. Badawi and Gh. Eshaq, *Ultrason. Sonochem.*, 2014, **21**, 1358–1365.
19 K. Rusevova, R. Köferstein, M. Rosell, H.H. Richnow, F.D. Kopinke and A. Georgi, *Chem. Eng. J.*, 2014, **239**, 322–331.
20 R.C.C. Costa, M.F.F. Lelis, L.C.A. Oliveira, J.D. Fabris, J.D. Ardisson, R.R.V.A. Rios, C.N. Silva and R.M. Lago, *J. Hazard. Mater.,* 2006, **129**, 171–178.
21 L.J. Xu, W. Chu and L. Gan, *Chem. Eng. J.*, 2015, **263**, 435–443.
22 X.G. Liu, N.D. Wu, C.Y. Cui, N.N. Bi and Y.P. Sun, *RSC Adv.*, 2015, **5**, 24016–24022.
23 Y.F. Han, F.X. Chen, Z.Y. Zhong, K. Ramesh, L.W. Chen, D. Jian and W.W. Ling, *Chem. Eng. J.*, 2007, **134**, 276–281.
24 W.X. Zhang, Z.H. Yang, X. Wang, Y.C. Zhang, X.G. Wen and S.H. Yang, **Catal. Commun.**, 2006, **7**, 408–412.
25 J. Zhao, J.J. Yang and J. Ma, *Chem. Eng. J.*, 2014, **239**, 171–177.
26 Y.H. Jo, W.C. Young and S.H. Do, *Ann. Int. Conference on*

Sustainable Energy Environ., 2013, 116.
27 Y.J. Yao, Y.M. Cai, F. Lu, F.Y. Wei, X.Y. Wang, S.B. Wang, *J. Hazard. Mater*., 2014, **270**, 61–70.
28 S.R. Pouran, A.A.A. Raman and W.M.A.W. Daud, *J. Clean. Prod.*, 2014, **64**, 24–35.
29 X.J. Yao, F. Gao and L. Dong, *Chin. J. Catal.*, 2013, **34**, 1975–1985.
30 H. Cheng, S.J. Chou, S.S. Chen and C.J. Yu, *J. Environ. Sci.*, 2014, **26**, 1307–1312 .
31 L. Hua, H.R. Ma and L. Zhang, *Chemosphere*, 2013, **90**,143–149.
32 H. Tajizadegan, M. Jafari, M. Rashidzadeh and A. Saffar-Teluri, *Appl. Surf. Sci.*, 2013, **276**, 317– 322.
33 L.F. Liotta, M. Gruttadauria, G. Di Carlo, G. Perrini and V. Librando, *J. Hazard. Mater.*, 2009, **162**, 588–606.
34 J.C. Zhang, Y.H. Wang and D.Y. Wu, *Energy Convers. Manage.*, 2003, **44**, 357–367.
35 H. Lin, H. Zhang, X. Wang, L.G. Wang and J. Wu. *Sep. Purif. Technol*., 2014, **122**, 533–540.
36 H.Y. Li, R. Priambodo, Y. Wang, H. Zhang and Y.H. Huang, *J. Tai Wan Inst. Chem. Eng.* 2015, **53**, 68–73.
37 J.H.Yi, Y.Y. Sun, J.F. Gao and C.Y. Xu, *T. nonferr. Metal. Soci.*, 2009, **19**, 1237–1242.
38 J.M. Fang, X.Y. Huang, X. Ouyang and X. Wang, *Chem. Eng. J.,* 2015, **270**, 309–319.
39 C.M. Chen, J. Wu, B.A. Yoza, Q.X. Li and G. Wang, *J. Environ. Manage.*, 2015, **152**, 58–65.
40 Z.C. Ma, X.Y. Wei, S.T. Xing and J.S. Li, *Catal. Commun.* 2015, **67**, 68–71.
41 Y.F. Han, F.X. Chen, K. Ramesh, Z.Y. Zhong, E. Widjaja and L.W. Chen, *Appl. Catal. B: Environ*., 2007, **76**, 227–234
42 P. Mahamallik, S. Saha and A. Pal, *Chem. Eng. J.*, 2015, **276,** 155–165.
43 E. Eren, H. Gumus and A. Sarihan, *Desalination*, 2011, **279**, 75–85.
44 S.M. Hoque, C. Srivastava, N. Srivastava, N. Venkateshan and K. Chattopadhyay, *J. Mater. Sci.* 2013, **48**, 812–818.
45 S. Sabale, V. Jadhav, V. Khot, X.L. Zhu, M.L. Xin and H.X. Chen, *J. Mater. Sci: Mater. Med.,* 2015, **26**, 1–9.
46 M. Günay, A. Baykal and H. Sözeri, *J. Supercond. Nov. Magn*., 2012, **25**, 2415–2420.
47 L.X. Yang and Y.J. Zhu, *Mater. Res. Bull.* 2007, **42**, 159–164.
48 H.C. Lan, A.M. Wang, R.P. Liu, H.J. Liu and J.H. Qua, *J. Hazard. Mater.,* 2015, **285**, 167–172.
49 Q.Q. Chen, P.x. Wu, Z. Dang, N.W. Zhu, P. Li, J.H. Wu and X.D. Wang, *Sep. Purif. Technol.*, 2010, **71**, 315–323.
50 M.L. Rache, A.R. García, H.R. Zea, A.M.T. Silva, L.M. Madeira and J.H. Ramírez, *Appl. Catal. B: Environ.*, 2014, **146**,192– 200.
51 B.H.J. Bielski, D.E. Cabelli, R.L. Arudi and A.B. Ross, *J. Phys. Chem. Ref. Data*, 1985, **14**, 1041–1098.
52 B.G. Kwon, D.S. Lee, N. Kang and J. Yoon, *Water Res.*, 1999, **33**, 2110– 2118.
53 M.H. Zhou, Q.H. Yu, L.C. Lei and G. Barton, *Sep. Purif. Technol*., 2007, **57**, 380–387.
54 T. Zhang, C.j. Li, J. Ma, H. Tian and Z.M. Qiang, *Appl. Catal. B: Environ.*, 2008, **82**, 131–137.
55 H. Zhang, H. Fu and D.B. Zhang, *J. Hazard. Mater*., 2009, **172**, 654–660.
56 G. Ersöz, *Appl. Catal. B: Environ.*, 2014, **147**, 353– 358.
57 Y. Wang, R. Priambodo, H. Zhang and Y.H. Huang, *RSC Adv.*, 2015, **5**, 45276–45283.
58 C.C. Amorim, M.M.D. Leão, R.F.P.M. Moreira, J.D. Fabris and A.B. Henriques, *Chem. Eng. J*., 2013, **224**, 59–66.
59 H. Zhang, F. Liu, X.G. Wu, J.H. Zhang and D.B. Zhang, *Asia-Pac. J. Chem. Eng*., 2009, **4**, 568–573..
60 J.H. Ramirez, C.A. Costa and L.M. Madeira, *Catal. Today*, 2005, **107–108**, 68–76.
61 J. Feng, X. Hu, P.L. Yue, H.Y. Zhu and G.Q. Lu, *Ind. Eng. Chem. Res*., 2003, **42**, 2058–2066.

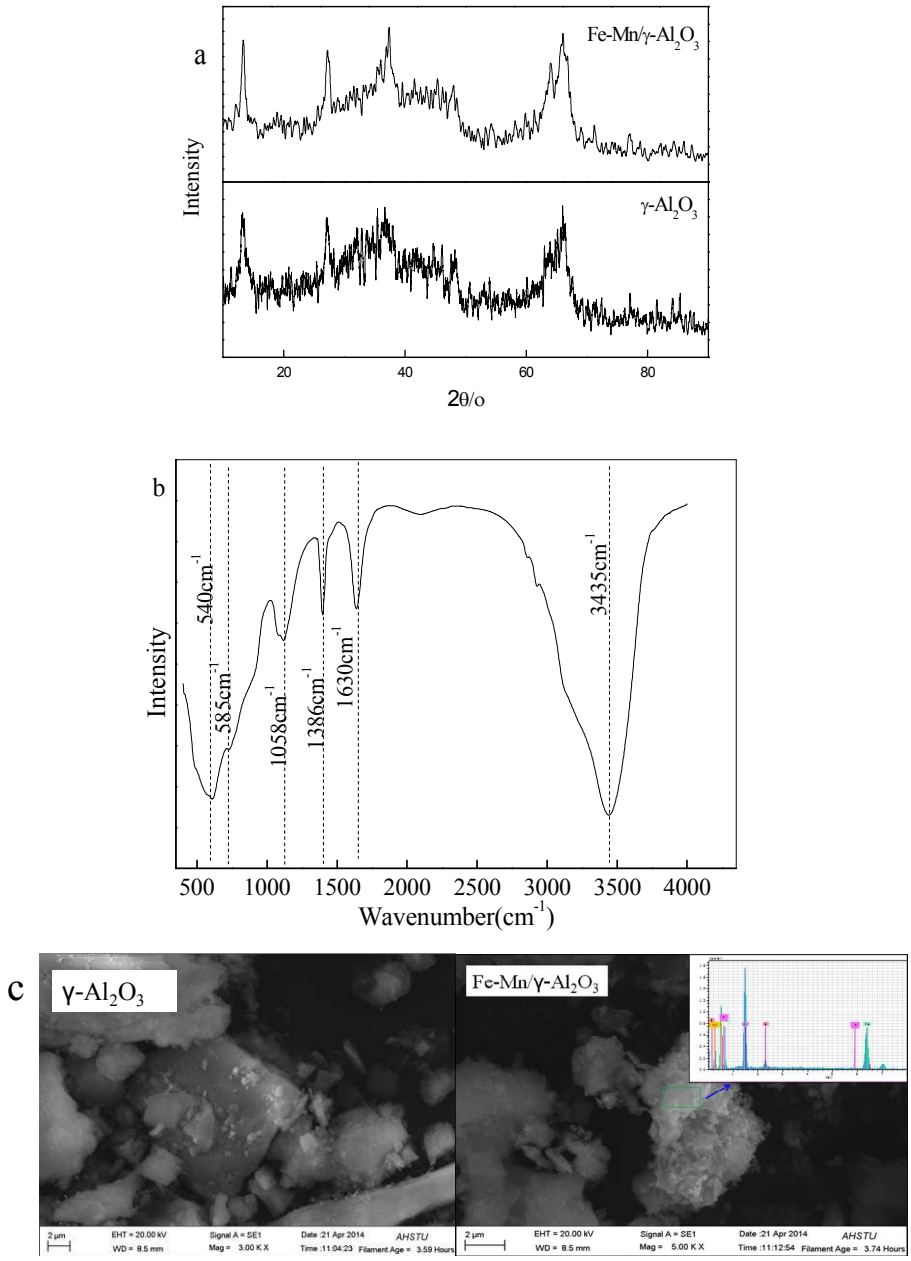

Fig. 1. (a) XRD pattern of γ-Al_2O_3 and Fe-Mn/γ-Al_2O_3, (b) FTIR spectra of Fe-Mn/γ-Al_2O_3 (c) SEM images of γ-Al_2O_3 and SEM images with EDS of Fe-Mn/γ-Al_2O_3.

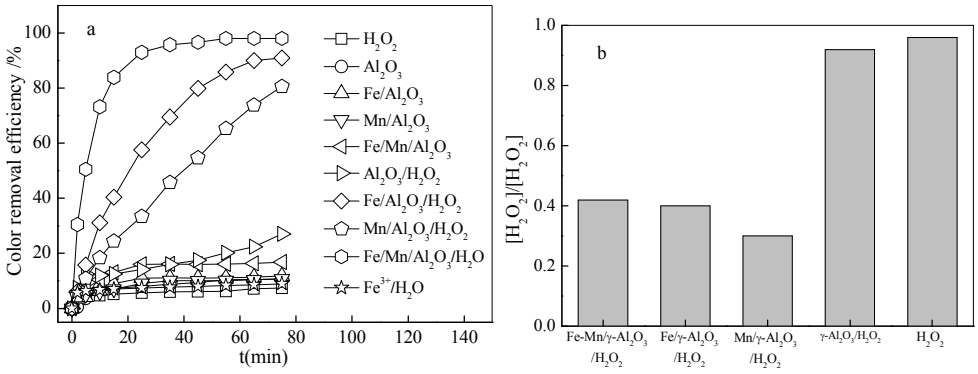

Fig. 2. (a) Degradation of RB5 under different conditions, (b) the remaining percentages of H_2O_2 ([RB5] = 50 mg L^{-1}, [H_2O_2] = 7 mmol L^{-1}, pH = 3, [Fe-Mn/γ-Al_2O_3] = 2.5 g L^{-1}).

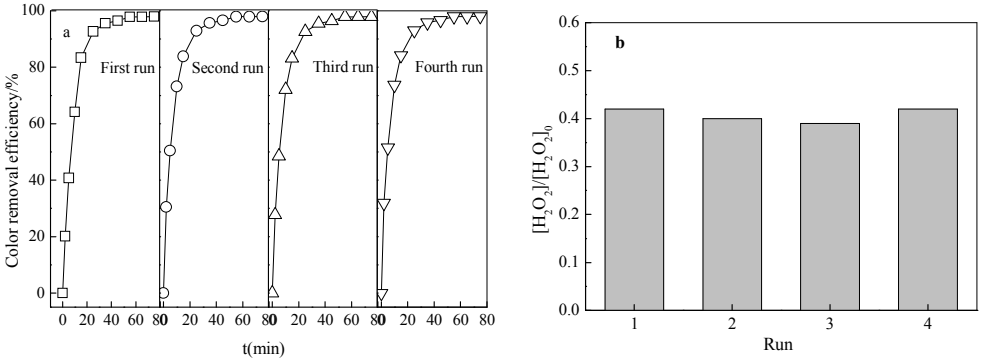

Fig. 3. (a) The reusability of Fe-Mn/γ-Al_2O_3, (b) the remaining percentages of H_2O_2 ([RB5] = 50 mg L^{-1}, [H_2O_2] = 7 mmol L^{-1}, pH = 3, [Fe-Mn/γ-Al_2O_3] = 2.5 g L^{-1}).

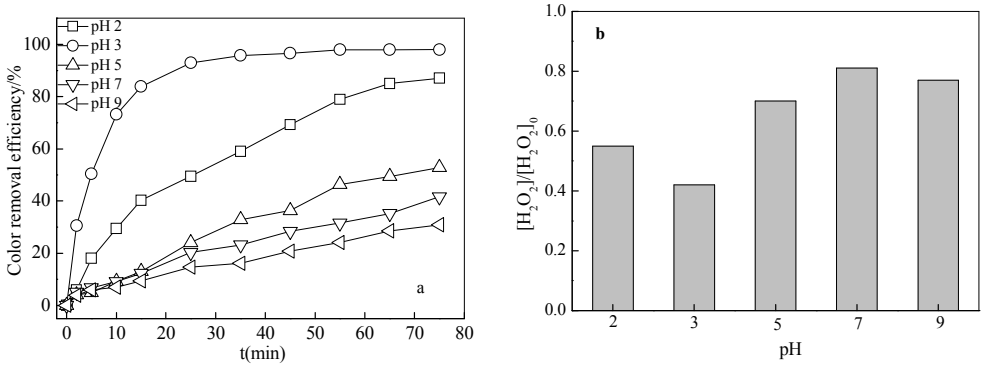

Fig. 4. (a) effect of pH on the RB5 decolorization, (b) the remaining percentages of H_2O_2 ([RB5] = 50 mg L^{-1}, [H_2O_2] = 7 mmol L^{-1}, [Fe-Mn/γ-Al_2O_3] = 2.5 g L^{-1}).

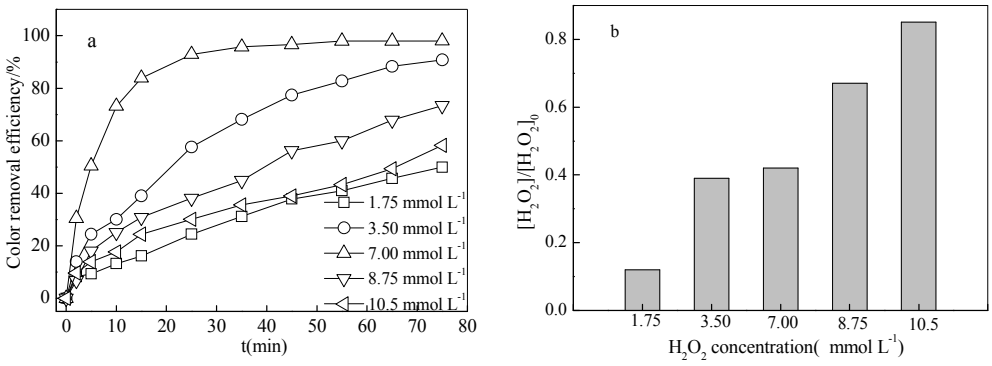

Fig. 5. (a) effect of H_2O_2 concentration on the RB5 decolorization, (b) the remaining percentages of H_2O_2 ([RB5] = 50 mg L^{-1}, pH = 3, [Fe-Mn/γ-Al_2O_3] = 2.5 g L^{-1}).

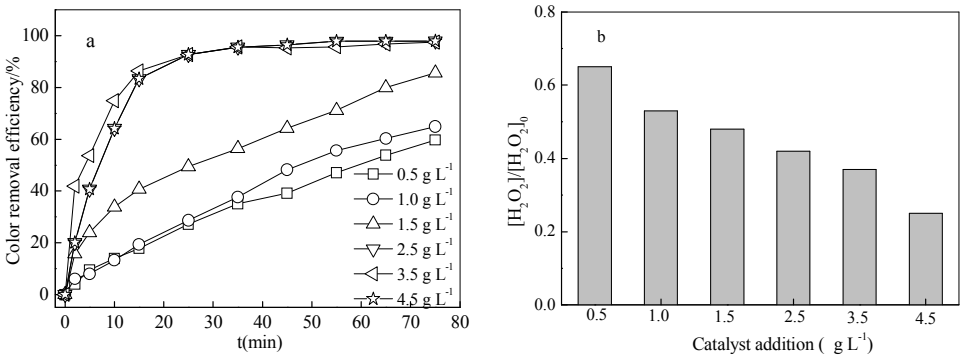

Fig. 6. (a) effect of catalyst addition on the RB5 decolorization, (b) the remaining percentages of H_2O_2 ([RB5] = 50 mg L^{-1}, [H_2O_2] = 7 mmol L^{-1}, pH = 3).

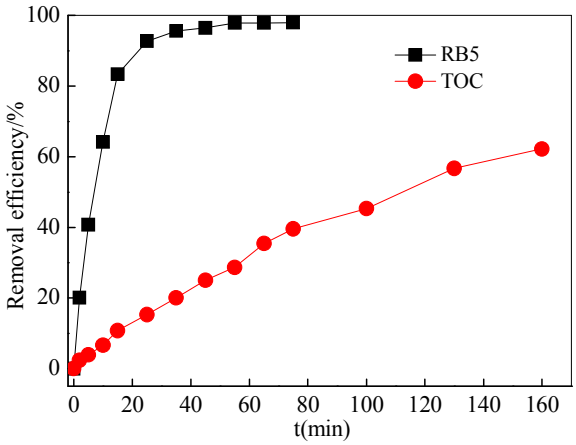

Fig. 7. The decolorization and mineralization of RB5 with reaction time ([RB5] = 50 mg L^{-1}, [H_2O_2] = 7 mmol L^{-1}, pH = 3, [Fe-Mn/γ-Al_2O_3] = 2.5 g L^{-1}).

Table 1
The surface atomic composition of Fe-Mn/γ-Al_2O_3

Element	Weight %	Atomic %
O	33.75	43.12
C	19.21	32.73
Fe	20.40	7.45
Al	16.66	12.62
S	1.78	1.06
Mn	8.20	3.05

Graphical abstract